Atmos. Chem. Phys. Discuss., 9, 15827–15865, 2009 www.atmos-chem-phys-discuss.net/9/15827/2009/© Author(s) 2009. This work is distributed under the Creative Commons Attribution 3.0 License.



This discussion paper is/has been under review for the journal *Atmospheric Chemistry* and *Physics (ACP)*. Please refer to the corresponding final paper in *ACP* if available.

Heterogeneous freezing of droplets with immersed mineral dust particles — measurements and parameterization

D. Niedermeier¹, S. Hartmann¹, R. A. Shaw^{1,2}, D. Covert³, Th. F. Mentel⁴, J. Schneider⁵, L. Poulain¹, P. Reitz^{5,6}, C. Spindler⁴, T. Clauss¹, A. Kiselev¹, E. Hallbauer¹, H. Wex¹, K. Mildenberger¹, and F. Stratmann¹

Received: 16 July 2009 - Accepted: 17 July 2009 - Published: 24 July 2009

Correspondence to: D. Niedermeier (niederm@tropos.de)

Published by Copernicus Publications on behalf of the European Geosciences Union.

ACPD

9, 15827–15865, 2009

Measurements and parameterization of immersion freezing

D. Niedermeier et al.

Title Page Introduction Abstract Conclusions References **Figures** Tables Back Close Full Screen / Esc Printer-friendly Version Interactive Discussion



¹Leibniz Institute for Tropospheric Research, 04318 Leipzig, Germany

²Dept. of Physics, Michigan Technological University, Houghton, MI 49931, USA

³University of Washington, Seattle, WA 98195, USA

⁴Forschungszentrum Jülich, 52425 Jülich, Germany

⁵Max Planck Institute for Chemistry, 55128 Mainz, Germany

⁶Institute for Atmospheric Physics, Johannes Gutenberg University, 55128 Mainz, Germany

Abstract

During the measurement campaign FROST (FReezing Of duST), LACIS (Leipzig Aerosol Cloud Interaction Simulator) was used to investigate the immersion freezing behavior of coated and uncoated Arizona Test Dust (ATD) particles with a mobility diameter of 300 nm. Particles were coated with succinic acid ($C_4H_6O_4$), sulfuric acid (H_2SO_4) , two different coating conditions), and ammonium sulfate $((NH_4)_2SO_4)$. Ice fractions at temperatures between 233.15 K and 240.65 K were determined for all types of particles acting as IN (Ice Nuclei). In this temperature range, uncoated particles and those coated with C₄H₆O₄ or small amounts of H₂SO₄ started to act as IN at higher temperatures compared to particles with larger amounts of H₂SO₄ or (NH₄)₂SO₄ coatings. Although the latter two showed similar hygroscopic growth and droplet activation behavior, they differed in their ability to act as IN. ATD particles coated with (NH₄)₂SO₄ were the most inefficient IN. The ability of the investigated particles to act as IN was found not to be related to water activity for the freezing process investigated, however, in LACIS, the supercooled droplets were activated and highly diluted before the freezing occurred. Applying the measurement results, a parameterization, based on a simplified CNT (Classical Nucleation Theory) type nucleation rate expression, was developed. The simplified theory allows us to determine that thermodynamic changes at the surface are dominating the change in nucleating ability, rather than changes in surface area or kinetic effects.

Introduction

Ice containing clouds, such as cirrus and mixed phase clouds have an impact on radiative balance by scattering and absorbing solar and terrestrial radiation (Hung et al., 2003; Zuberi et al., 2002), and through ice formation processes cloud radiative properties are changed (DeMott et al., 2003b). Additionally, the formation of ice crystals in clouds affects cloud dynamics and chemical processes and is one of the most effec-

ACPD

9, 15827–15865, 2009

Measurements and parameterization of immersion freezing

D. Niedermeier et al.

Introduction

References

Figures

Close

Title Page Abstract Conclusions Tables Back Full Screen / Esc Printer-friendly Version



Interactive Discussion

tive pathways to form precipitation particles in the midlatitudes. Therefore, ice particles largely affect cloud lifetime (Lohmann, 2006).

Ice formation in the atmosphere may happen via homogeneous nucleation, but it often occurs by heterogeneous nucleation, with the nucleation event being induced by 5 a foreign insoluble substance called an ice-forming nucleus (IN) (Cantrell and Heymsfield, 2005). Four different heterogeneous freezing modes are distinguished in the literature: Deposition, condensation, immersion and contact freezing mode (e.g., Pruppacher and Klett, 1997). In the deposition mode, ice deposits on the particle directly from the vapor phase, without an intermediate liquid stage. That means the particle environment is super-saturated with respect to ice and sub-saturated with respect to liquid water. Condensation freezing occurs when the particle acts as cloud condensation nucleus (CCN) at a certain temperature below the melting point of water and the freezing process takes place at the same temperature during the condensation process. For immersion freezing, Pruppacher and Klett (1997) stated that the particle becomes immersed into a droplet above the melting point and freezing is initiated when the temperature of this droplet becomes sufficiently low. But evidence exists that immersion freezing may also occur if the particle becomes immersed into the liquid droplet below the melting point temperature or acts as CCN below 273.15 K. Due to further cooling, the particle will then induce the freezing (Megahed, 2007). This definition will be used for LACIS data interpretation. Last but not least, freezing can also be initiated by an insoluble particle which penetrates the surface of a supercooled liquid droplet from the outside. This so-called contact freezing apparently could also occur if the particle penetrates the droplet surface from the inside due to particle movement or an evaporation process (Shaw et al., 2005; Durant and Shaw, 2005).

The relative importance of the freezing modes in the atmosphere is poorly known. The occurrence of some modes is discussed controversially and partly doubted. For example, Meyers et al. (1992) suggest that deposition nucleation occurs at water supersaturated conditions, too. Therefore, it is difficult to distinguish between freezing in deposition and condensation modes and the question remains if condensation freez-

ACPD

9, 15827–15865, 2009

Measurements and parameterization of immersion freezing



ing takes place in the atmosphere at all. In general, our understanding of physical and chemical processes underlying heterogeneous ice formation is limited. Therefore, more scientific work, both theoretical and experimental, is necessary to elucidate fundamental physical mechanisms, as well as to develop adequate parameterizations that are required for cloud models (Cantrell and Heymsfield, 2005; Kärcher and Lohmann, 2003).

Various atmospheric observations of droplet freezing through heterogeneous ice nucleation show that insoluble substances, especially mineral dust particles, serve effectively as IN in the atmosphere (Cziczo et al., 2004; DeMott et al., 2003a,b; Richardson et al., 2007; Sassen et al., 2003). As a result mineral dust particles indirectly influence cloud properties, precipitation, and therefore earth's climate (DeMott et al., 2003a,b; Zuberi et al., 2002). Mineral dust particles originate from desert regions like the Sahara and the Gobi and can be lifted into the free troposphere during storm events. Subsequent to lifting, the dust particles can be transported over large distances (Prospero, 1999; Sassen et al., 2003; DeMott et al., 2003a) and undergo aging processes, e.g., through coatings with sulfates and other electrolytes (Zuberi et al., 2002). As a result IN ability may change.

In the laboratory several investigations concerning the IN ability of different kinds of mineral dust particles (with and without coatings) were carried out utilizing a variety of measurement methods and thermodynamic conditions (Archuleta et al., 2005; Field et al., 2006; Knopf and Koop, 2006; Marcolli et al., 2007; Möhler et al., 2006; Zobrist et al., 2008). As a consequence, our understanding of the influence of certain particles, especially mineral dusts, on different freezing modes has improved. Nevertheless, the studies possessed some limitations, some of which we have attempted to address in this work. In some cases only freezing onset thresholds are given (Archuleta et al., 2005; Field et al., 2006; Möhler et al., 2006). In other cases the IN ability of broad particle size distributions was investigated (Field et al., 2006; Knopf and Koop, 2006; Marcolli et al., 2007; Möhler et al., 2006; Zobrist et al., 2008) providing little information about the influence of particle size on freezing. Taken together, the studies are partly

ACPD

9, 15827–15865, 2009

Measurements and parameterization of immersion freezing





difficult to compare, and even when certain results can be compared they are partly contradictory and not entirely consistent. Further research is necessary, and here we address the IN efficiency of size segregated particles of known chemical composition in the immersion freezing mode. Since ice fractions, i.e. the number of frozen droplets per total number, determined using different measurement devices, are not comparable (e.g. due to different residence times inside the different instruments), we are careful to obtain nucleation rates which are not instrument specific and therefore generally comparable.

During the measurement campaign FROST (FReezing Of duST) which took place in April 2008, the laminar flow diffusion chamber LACIS (Leipzig Aerosol Cloud Interaction Simulator) (Stratmann et al., 2004) was extended to investigate the ability of mineral dust particles to act as IN. These were the first measurements of heterogenous freezing performed with LACIS. LACIS allows the investigation of immersion freezing, such that the influence of size segregated particles on the freezing behavior of droplets can be measured, where only one particle is immersed in each droplet. LACIS can be used to determine ice fractions as function of temperatures from which nucleation rates can be derived.

Arizona Test Dust (ATD) was used as a surrogate for mineral dust for the freezing experiments during the FROST campaign. To simulate aging processes, the ATD particles were coated with various substances such as ammonium sulfate ((NH₄)₂SO₄), sulfuric acid (H₂SO₄, two different coating conditions) and succinic acid (C₄H₆O₄). The coating amounts are in the range observed in the atmosphere (Mertes et al., 2005; Yuskiewicz et al., 1999)

For freezing experiments a narrow particle size distribution with a mobility diameter of 300 nm was chosen. Additional instrumentation was used to characterize the selected particles with respect to shape, chemical composition, hygroscopic growth and droplet activation (Wex et al., 2009; Reitz et al., 2009). In LACIS, various temperature values between 233.15 K and 240.65 K were set and the corresponding ice fractions were obtained. Assuming a stochastic nature of the freezing process, a parameterization,

ACPD

9, 15827–15865, 2009

Measurements and parameterization of immersion freezing





based on a classical nucleation theory (CNT) type rate expression, has been developed to quantify the immersion freezing behavior of the investigated particles.

Theoretical approach for data interpretation and parameterization

CNT is far from serving as an accurate description of nucleation processes, on the one side due to uncertainties in the required parameters, and on the other side due to questionable assumptions underlying the theory itself. Nevertheless, it can be used at least in a phenomenological way to interpret observations (Shaw et al., 2005). For example, CNT provides a feasible method to parameterize homogenous and heterogeneous ice nucleation as function of temperature.

For heterogenous freezing the nucleation rate coefficient j_{het} can be expressed as (Pruppacher and Klett, 1997):

$$j_{\text{het}}(T) = \frac{kT}{h} \exp\left[-\frac{\Delta F(T)}{kT}\right] \times n_{\text{s}} \exp\left[-\frac{\Delta G_{\text{het}}(T)}{kT}\right]$$
(1)

where h and k are the Planck and Boltzmann constants, respectively. T represents the absolute temperature and n_s is the number density of water molecules at the ice nucleus/water interface. $\Delta F(T)$ is the activation energy for diffusion of water molecules crossing the liquid-water/ice boundary. $\Delta G_{het}(T)$ represents the Gibbs free energy for critical ice embryo formation in the presence of an IN. In general, the first term in Eq. (1) essentially describes the flux of water molecules to the embryonic ice particles (kinetic effect) and the second term presents the equilibrium number of critical embryos in the liquid phase (thermodynamic effect) (e.g., Shaw et al., 2005).

Using the simplest spherical cap geometry for the ice germ, the Gibbs free energy $\Delta G_{\text{het}}(T)$ can be written as (Seinfeld and Pandis, 1998):

$$\Delta G_{\text{het}}(T) = \frac{16\pi v_i^2(T)\sigma_{\text{W,i}}^3(T)}{3\left(kT \ln \frac{\rho_{\text{w}}(T)}{\rho_i(T)}\right)^2} f_{\text{het}}$$
(2)

ACPD

9, 15827-15865, 2009

Measurements and parameterization of immersion freezing

D. Niedermeier et al.

Introduction

References

Figures

Close

Title Page Abstract Conclusions Tables Back Full Screen / Esc Printer-friendly Version



Interactive Discussion

with $v_i(T)$ being the volume per water molecule in the ice phase, $\sigma_{w_i}(T)$ being the interfacial free energy between liquid water and the ice embryo. f_{het} represents the reduction of the energy barrier in consequence of the IN presence. $p_w(T)$ and $p_i(T)$ are the vapor pressures of supercooled liquid water and ice, respectively. The strongest temperature dependencies in Eq. (2) are in the vapor pressures and the surface free energy, so we proceed by focusing on those two terms. The ratio $p_w(T)/p_i(T)$, representing the saturation ratio, can be written as (e.g., Rogers and Yau, 1996):

$$\frac{\rho_{\rm w}(T)}{\rho_{\rm i}(T)} = \exp\left(\frac{I_{\rm f}}{kT} \frac{T_{\rm s}}{T_{\rm o}}\right) \tag{3}$$

where $I_{\rm f}$ is the molecular latent heat of fusion, $T_{\rm o}$ is the melting point temperature, and $T_s \equiv T_s - T$ is the supercooling temperature.

The surface free energy $\sigma_{w,i}(T)$ can also be expressed in terms of T_s , which we obtain by adapting the expression of Zobrist et al. (2007) $(\sigma_{w,i}(T) = \tilde{\sigma}_{w,i} [1 - (T_s/C_1)]$, valid for 230 K $\leq T \leq$ 244 K) with $\tilde{\sigma}_{wi} = 0.0412 \,\mathrm{Jm}^{-2}$ and $C_1 = 82.4 \,\mathrm{K}$. Given that the absolute temperature T does not change significantly (FROST measurements were performed within a temperature range <10 K), we can reasonably take ΔF , I_f and v_i as constants for the investigated temperature range. Using Eqs. (2) and (3) and the stated assumptions, j_{het} can be written as:

$$j_{\text{het}}(T_{\text{S}}) = a' \times \exp \left[-\frac{C_2 \left(1 - \frac{T_{\text{S}}}{C_1} \right)^3}{T_{\text{S}}^2} f_{\text{het}} \right]$$
(4)

with $a' = kT n_s \exp(-\Delta F(T)/kT) / h$ and $C_2 = 16\pi v_i^2 T_o^2 \tilde{\sigma}_{w_i}^3 / 3kT I_f^2$.

In the following, this CNT based nucleation rate coefficient will be connected to the ice fraction (i.e. the number of frozen droplets per total number N_0), which is the property that was measured with LACIS during FROST. Here we took advantage of the fact that inside LACIS only one IN is present per droplet. Because of the narrow particle

ACPD

9, 15827-15865, 2009

Measurements and parameterization of immersion freezing

D. Niedermeier et al.

Introduction

References

Figures

Close

Interactive Discussion

Title Page Abstract Conclusions Tables Back Full Screen / Esc Printer-friendly Version size distribution of the ATD particles (see Wex et al., 2009), it will be assumed that the particles feature a similar size, a similar surface and similar surface properties. In addition, the nucleation event in an individual droplet is assumed to be independent of the nucleation event in other droplets of the population and the ice formation is the consequence of only one nucleation event per droplet (Pruppacher and Klett, 1997). The last assumption is reasonable because of the fast crystallization velocity of water. Hence, it is likely that the first critical embryo, formed on the particle surface, initiates the freezing before further embryos can be formed. This is a consequence of the latent heat release during the phase transition, such that the temperature within the droplet suddenly increases.

Under these assumptions the following equation can be written:

$$\frac{dN_{\rm u}}{dt} = -N_{\rm u} s_{\rm p} j_{\rm het}(T_{\rm s}) \tag{5}$$

with $dN_u = -dN_f$. Here, s_p is the particle surface area, and N_u and N_f are the number of unfrozen and frozen particles, respectively. Integrating Eq. (5) from the total number N_0 at t=0 to N_u at t and considering that T_s depends on t because of the temperature profile inside LACIS (Hartmann et al., 2009)), it can be derived:

$$f_{\text{ice}} = \frac{N_{\text{f}}}{N_{0}} = 1 - \exp\left(-s_{\text{p}} \int_{0}^{t} j_{\text{het}}(T_{\text{s}}(t')) dt'\right)$$
 (6)

where f_{ice} represents the ice fraction, or the probability of freezing (Shaw et al., 2005). For the FROST setup the major part of ice is formed in a region inside LACIS where the supercooling temperature, and therefore j_{het} , is almost constant (Hartmann et al., 2009). Eq. (6) therefore simplifies to:

$$f_{\text{ice}} = 1 - \exp\left(-s_{\text{p}}j_{\text{het}}(T_{\text{s}})t\right) \tag{7}$$

ACPD

9, 15827–15865, 2009

Measurements and parameterization of immersion freezing

D. Niedermeier et al.

Title Page

Abstract Introduction

Conclusions References

Tables Figures

I ◀ ▶I

■ Back Close

Full Screen / Esc

Printer-friendly Version

Interactive Discussion



Finally, Eq. (4) can be inserted into Eq. (7) resulting in:

$$f_{\text{ice}} = 1 - \exp\left(-a \times \exp\left(-\frac{C_2\left(1 - \frac{T_s}{C_1}\right)^3}{T_s^2}f_{\text{het}}\right)t\right)$$
 (8)

valid for $29 \, \text{K} \le T_{\text{s}} < 38 \, \text{K}$. Here, $a = a' s_{\text{p}}$ and f_{het} are left as fitting parameters for the immersion freezing. Parameter a includes information about the total particle surface area and kinetic effects, whereas f_{het} contains information about surface properties and thermodynamic effects.

3 Experimental procedure

3.1 Particle generation and size selection

Figure 1 shows the particle generation setup. The ATD particles (ISO 12103-1, A1 Ultrafine Test Dust, Powder Technology Inc., Burnsville, Minnesota, USA) were dispersed by means of a fluidized bed generator (TSI 3400A, TSI Inc., St. Paul, Minnesota, USA). As a result of friction in the fluidized bed the particles are multiply charged and a self-built Corona discharger is used to discharge them partially. Then, particles with an aerodynamic diameter larger than 560 nm were removed from the aerosol flow by means of a Micro-Orifice Uniform-Deposit Impactor (MOUDI Model 100R, MSP Corporation, Shoreview, Michigan, USA). The remaining particles were charged electrically by means of a Krypton 85 neutralizer. Coatings were applied in vapor diffusion tubes, heated to suited temperatures. The first tube (A) shown in Fig. 1 is a bypass section where the uncoated particles were led through. The second tube (B) contained a small "boat" filled with $C_4H_6O_4$. This tube was heated up to 80°C using a heating tape. The temperature stability of this tape was about ± 2 K. As a result of the heating the $C_4H_6O_4$ was vaporized from the "boat" and the vapor condensed on the ATD particles in the cooler section downstream of the heated tube. The third tube (C) contained a

ACPD

9, 15827–15865, 2009

Measurements and parameterization of immersion freezing

D. Niedermeier et al.



15835

"boat" filled with H_2SO_4 . This tube was surrounded by a water jacket the temperature of which was controlled by a thermostat (HAAKE C25P, HAAKE GmbH, Karlsruhe, Germany). Two temperature values were adjusted during different experiments (50°C and 70°C) resulting in two different amounts of H_2SO_4 on the particles. The temperature stability was ± 0.1 K. To generate the (NH₄)₂SO₄ coating, the ATD particles were first led through the H_2SO_4 tube heated to 70°C. Then, the particles were passed over a water bath. The aerosol here was humidified to dew-point temperature similar to the laboratory temperature of about 25°C. Then, ammonia gas was added. On a three meter reaction path the neutralization of the particulate H_2SO_4 by the ammonia gas took place. After that the aerosol flow was dried using a diffusion dryer.

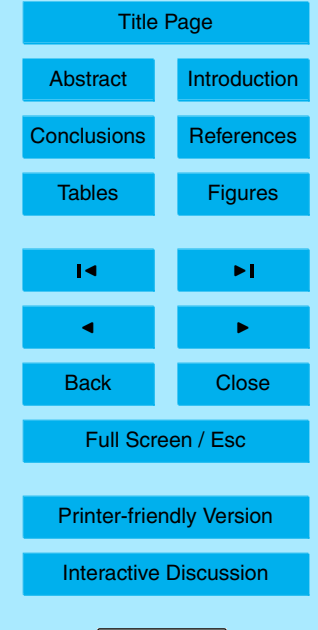
Downstream the coating device, a DMA (Differential Mobility Analyzer; Knutson and Whitby (1975); type "Vienna Medium") was used to select a quasi-monodisperse particle size fraction. For the freezing experiments, particles with a mobility diameter $D_{\rm mob}$ of 300 nm were selected.

Downstream of the DMA the aerosol flow was split by a flow divider with one fraction (0.66 l min⁻¹) being directly fed to three Aerosol Mass Spectrometers (AMS, from IFT, Research Center Jülich, Germany and University of Mainz, Germany). The other fraction (0.34 l min⁻¹) was lead to a dilution system where particle free air (1.5 l min⁻¹) was added. All flows were controlled by mass flow controllers (MKS 1179, MKS Instruments Deutschland GmbH, Munich, Germany) and checked on a daily basis with a bubble flow meter (Gilian® GilibratorTM2, Sensidyne Inc., Clearwater, Florida, USA). From here, the remaining instruments (Condensation Particle Counter (CPC, GRIMM 5.304, GRIMM Aerosol Technik GmbH & Co. KG, Ainring, Germany); Cloud Condensation Nucleus Counter (CCNC, DMT, Boulder, Colorado, USA, Roberts and Nenes, 2005), High-Humidity Tandem Differential Mobility Analyzer (HH-TDMA, Hennig et al., 2005) and LACIS) were fed with the required flows. For LACIS measurements an aerosol flow of 0.08 l min⁻¹ was used.

ACPD

9, 15827–15865, 2009

Measurements and parameterization of immersion freezing





3.2 LACIS-measurement procedure and data evaluation

During FROST, the first heterogenous freezing measurements at LACIS were performed. Therefore, a straightforward and simple measurement setup was used.

The aerosol flow entered LACIS (Fig. 2) with a dew-point temperature of about 233.15 K. A part of particle free sheath air flow was humidified by a saturator (Perma Pure PH-30T- 24KS, Perma Pure LLC, Toms River, New Jersey, USA) and subsequently mixed with a dry particle free air flow resulting in a dew-point temperature of 266.15 K. This dew-point temperature was monitored using a dew-point mirror (DPM, Dew Prime I-S2, Edge Tech, Milford, Massachusetts, USA) measuring with an accuracy of ±0.1 K.

The dry aerosol and sheath air flows were combined in the inlet section of LACIS. The aerosol was confined by the sheath air to a narrow beam (about 2 mm in diameter) at the center axis of LACIS. The volume flow rates of sheath air and aerosol flow were chosen such that both flows entered LACIS in an isokinetic fashion with a velocity of about 0.4 m s⁻¹.

LACIS itself is a laminar flow tube with a diameter of 15 mm. It consists of seven 1 m tubes, each surrounded by a thermostated water-jacket (thermostats 1 to 5: JULABO FP50, JULABO Labortechnik GmbH, Seelbach, Germany; thermostats 6 to 7: JULABO LH85) so that the temperature of each section can be controlled separately (Fig. 2).

For the detection of the particles at the outlet of LACIS, a white light aerosol spectrometer (WELAS® 1000, PALAS®, Karlsruhe, Germany) was used. Downstream of WELAS®, the particle concentration was measured by means of a CPC (TSI 3010, TSI Inc., St. Paul, Minnesota, USA). The outlet dew-point temperature was monitored using a DPM (MBW 973, MBW Calibration Ltd., Wettingen, Switzerland).

During FROST, the inlet temperature and the wall temperature of the first LACIS section were set to 293.15 K. The wall temperatures of section two to five were set to 273.15 K. During the experiments, which were performed under atmospheric pressure

ACPD

9, 15827–15865, 2009

Measurements and parameterization of immersion freezing



conditions, only the temperatures of Sects. 6 and 7 were adjusted in a range where freezing was observable. Here, two different measurement procedures were carried out. In the first case only Sect. 7 was cooled down to temperature values between 233.15 K and 240.65 K and Sect. 6 was kept at 273.15 K (one-section measurement). In the second case both sections (6 and 7) were cooled down to the same temperature ranging between 233.15 K and 240.65 K (two-section measurement). The residence time in the last two sections was about 3.1 s (the residence time in Sect. 7 was about 1.56 s). For wall temperatures below 273.15 K, the corresponding inner tube walls were coated with ice by cooling the respective tube(s) down to 233.15 K for 5 to 10 min prior to the measurements. This procedure was necessary to ensure well-defined and reproducible wall boundary conditions for both, the experiments themselves and the numerical simulations described in Hartmann et al. (2009).

The inlet conditions in combination with the wall temperatures determine the temperature and saturation profiles inside LACIS through the heat and water vapor transfer processes, the particle beam is exposed to in the center of the tube. As mentioned above, the inlet conditions and the wall temperature of the first five sections were fixed and only the temperatures for Sects. 6 and 7 were varied within the given interval. Therefore, the temperature and saturation profiles inside the tube and the resulting droplet/ice crystal growth processes and phase transition were controlled by the settings of these last two sections (Hartmann et al., 2009). In Fig. 3, model simulations of the droplet growth behavior inside the last two sections are presented for three different wall temperatures (233.15 K, 238.15 K and 239.15 K), using the Computational Fluid Dynamics (CFD) code FLUENT 6 (FLUENT, 2001) together with the Fine Particle Model (FPM) (Particle Dynamics, 2005). The boundary conditions for the simulations were equal to the experimental ones assuming the inner tube walls of Sects. 6 and 7 to be covered with ice. Ice formation in the droplet phase was not considered in the simulations. It should be noted that the model is not yet capable of describing LACIS in its full complexity and has therefore to be considered half quantitative. However useful insights into the processes taking place in LACIS can already be gained at the current

ACPD

9, 15827-15865, 2009

Measurements and parameterization of immersion freezing

D. Niedermeier et al.



Þ١

Close



stage.

The trajectories in Fig. 3 show for three wall temperature settings at which temperatures (temperature of particle/droplet beam) the water droplets are formed and which temperatures they experience during their growth and evaporation process while traveling (right to left) along the LACIS axis. In the hygroscopic growth regime, particle/droplet diameter is more or less constant. With the temperature decreasing further, particles/droplets become activated and grow dynamically, roughly until reaching the end of section one (marked with the black points). Further downstream droplets evaporate in various degrees: For a wall temperature of 239.15 K droplets evaporate and become deactivated towards the end of the second section (marked with a x). For a wall temperature of 238.15 K, the behavior is somewhat similar, but the droplets still survive, although they shrink significantly. For a wall temperature of 233.15 K, droplets only shrink to a small extend and leave LACIS as large activated droplets.

Looking at these trajectories it becomes obvious that in LACIS different freezing mechanisms, i.e., immersion freezing, deposition freezing, and evaporation freezing could occur. If the droplets reach temperatures below 235 K, even homogeneous freezing would be possible. An analysis concerning the actual freezing modes observed in LACIS during FROST will be given in Sect. 4. For more detailed information concerning the thermodynamic conditions and profiles for different settings at LACIS please refer to Hartmann et al. (2009).

The main goal of this study was to obtain ice fractions whereas knowing the correct size of the ice particles with large accuracy is less relevant. Under these circumstances WELAS® was an adequate device to meet the requirements, with two limitations. First, the distinction between seed particles (coated or uncoated ATD particles), supercooled water droplets and ice crystals is not straight forward. However, the optical signal which originates from the seed particles is smaller than signal resulting from the droplets/ice crystals and is clearly distinguishable from them. Under the given conditions inside LACIS, the spherical droplets activate and grow (or evaporate) to similar sizes resulting in a narrow size distribution. In contrast, the growth of the ice crystals results in non-

ACPD

9, 15827–15865, 2009

Measurements and parameterization of immersion freezing



spherical shapes, and leads to optically broader size distributions in comparison to the droplet mode. This is utilized to distinguish between droplets and ice particles.

Secondly, the counting efficiency of WELAS® is size dependent. The counting efficiency is close to 0 for the particles at the lower detection limit (about 300 nm for water droplets) and 1 for the particles above 1 μ m (this size corresponds to a WELAS® size channel >100). In the transition range the counting efficiency is a function of the scattering signal amplitude and should be corrected if accurate measurements of particle number concentrations are required. The necessary correction can be obtained by simultaneously measuring the number concentration of the particles of known size with a CPC and WELAS®. During the FROST experiment, analyzed particles occupied two clearly separated size ranges: small seed particles (coated and uncoated ATD particles detected at WELAS® size channels <100), and large water droplets and ice crystals with sizes larger than 1 μ m (detected at WELAS[®] size channels >100). This allowed for the application of a step-like correction function ignoring the transition region between the small and large particles. That means, to obtain the number of small seed particles a correction factor of $C_{\text{seed}} = 0.05 \pm 0.03$ has to be applied while for the large droplets/ice crystals a correction is not necessary. In order to compare the corrected seed particle and droplet/ice crystal number with the particle number measured by the CPC downstream of LACIS, a second correction has to be considered because the extension of the particle beam is larger than the WELAS® measuring volume. An experimentally determined correction factor $C_{\text{MV}} = 0.42 \pm 0.05$ was accounted for.

In order to calculate the ice fraction f_{ice} from a LACIS experiment, the number of ice crystals N_{f} has to be divided by the total number N_{0} (see Eq. 6) wherein N_{0} is obtained through:

$$N_0 = \frac{\frac{N_{\text{seed}}}{C_{\text{seed}}} + N_{\text{drop/ice}}}{C_{\text{MV}}}.$$
 (9)

Here, $N_{\rm seed}$ and $N_{\rm drop/ice}$ represent the uncorrected number of small seed particles and the number of large water droplets/ice crystals, respectively. All measured particles 15840

ACPD

9, 15827–15865, 2009

Measurements and parameterization of immersion freezing

D. Niedermeier et al.

Title Page



were corrected as described above. As a consistency check, N_0 determined from Eq. (9) was compared to the number counted by the CPC. Both numbers matched within measurement uncertainties for the different experiments.

In the following, a freezing experiment using pure ATD particles is presented, including one- and two-section measurements (see Fig. 4). First of all, from 14:15 to about 14:30 the last section was cooled down below 233.15 K to form ice on the inner tube wall. As a consequence the particle size increased starting with the seed particle mode and ending with a mixture of water droplets and ice crystals. After this preparation the experiment started at 14:35 with increasing the temperature to 243.15 K. Here, WELAS® detected the seed particles again. Then, the wall temperature was decreased in 2.5 K steps (14:45 to 15:05). At about 238.15 K and 235.65 K a very narrow size distribution at larger sizes is visible in the upper part of Fig. 4, implying the existence of supercooled water droplets. Additionally, a small ice mode can be seen. Below 233.15 K, the amount of ice increased intensely.

From about 15:05 to 15:25 Sect. 6 was cooled down below 233.15 K to form ice on the inner tube wall. This time range represents a transition region and therefore, WELAS® signals are not used for data interpretation. After this preparation the temperatures of the last two sections were set to the same value. For the low temperatures, a very broad distribution can be seen that is caused by ice crystals. With a stepwise increasing temperature the amount of ice crystals decreased and the seed particles reappeared, with increasing amount. At the end of the measurement the ice crystal mode completely disappeared.

In summary, three different particle modes appeared during a LACIS one-section measurement: seed mode, supercooled water droplet mode and ice crystal mode. The water droplet and the ice crystal mode overlap under some conditions (see Fig. 5), i.e., a clear distinction between these modes is difficult for one-section measurements and the determined ice fraction values have a large uncertainty. Therefore, this kind of measurement was not used for ice fraction determination. Nevertheless, these measurements show, that inside LACIS droplets are generated first which then start to freeze.

ACPD

9, 15827–15865, 2009

Measurements and parameterization of immersion freezing





Therefore, the one-section measurements provide insight into the freezing modes occurring inside the tube (see next section).

For two-section measurements, the supercooled droplets either freeze or evaporate due to the Wegener-Bergeron-Findeisen effect (Findeisen, 1938), caused by both the ice at the inner tube and the nucleated ice crystals. Therefore, the sharp droplet mode is absent and clearly distinguishable seed and ice crystal modes remain and only the respective number concentrations vary with changing wall temperatures. At the lowest temperature of 233.15 K only ice crystals were observed (see Fig. 6). This kind of measurement procedure was used to determine ice fractions for different temperature values. A bimodal log-normal fit procedure was performed to separate seed and ice crystal mode and to determine the number of seed particles and ice crystals.

4 Results and discussion

Figure 7 presents the ice fraction values using pure ATD particles as IN as a function of supercooling temperature ranging from 32.5 K to 40 K. Again, the supercooling temperature is defined as $T_s \equiv T_o - T$. Here, T corresponds to the adjusted wall temperature of the last two sections $T_{w.6-7}$.

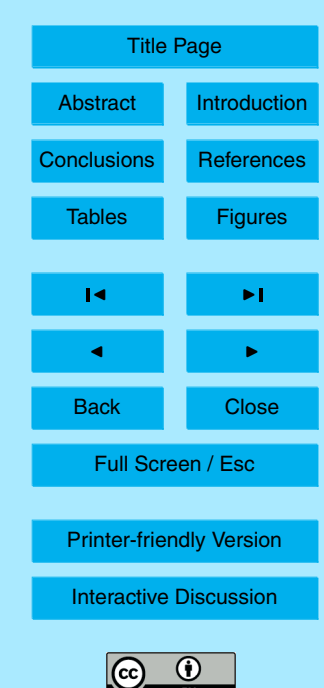
As mentioned above, the ice fraction values were obtained from the two-section measurements, after correction of the WELAS® size dependent counting efficiency (Eq. 9). Each data point was measured at least three times and the error bars represent the respective standard deviations.

Figure 7 shows that with increasing $T_{\rm s}$ the ice fraction increases monotonically, reaching a value of 1 at $T_{\rm s}$ =39 K. This behavior reflects the monotonic increase of nucleation rate with increasing supercooling. Due to the temperature profile inside LACIS, each data point represents an integrated ice fraction value from $T_{\rm o}$ to $T_{\rm s}$ at the end of the tube (see Hartmann et al., 2009). It should be noted that the ice fraction values for $T_{\rm s}$ <34 K are underestimated because the supercooled droplets evaporate before reaching the adjusted wall temperature (see Fig. 3). That means these values

ACPD

9, 15827–15865, 2009

Measurements and parameterization of immersion freezing



represent integrated ice fractions starting from T_{\circ} to a supercooling temperature less than T_{\circ} given in Fig. 7.

The question arises, which freezing modes do occur when running LACIS as described above. Since the measurements were performed for values of $T_{\rm s}$ up to 40 K, homogeneous freezing is most likely for the highest supercoolings. To verify this, homogeneous freezing of diluted ammonium sulfate solution droplets was studied using the FROST measurement setup. As a result, homogeneous freezing was clearly visible for $T_{\rm s} \ge 38$ K. Therefore, heterogeneous and homogeneous freezing are not distinguishable for $T_{\rm s} \ge 38$ K. These data points will be excluded in the later analysis.

A chance for deposition freezing to occur exists because over a short time the environment inside the tube compared to particle surface is supersaturated with respect to ice but subsaturated with respect to liquid water. To test if deposition freezing is likely or not, additional two-section experiments were performed. Here, LACIS conditions were adjusted such that the maximum saturation with respect to liquid water was always below 1, but saturation with respect to ice was above 1. These additional experiments were performed for two different inlet dew-points (265.95 K and 260.15 K) to detect possible deposition freezing in two different temperature intervals (from T_s =28 K to 30 K for dew-point of 265.95 K and from T_s =36 K to 38 K for dew-point of 260.15 K, see Fig. 8). For the lower supercooling temperature interval no deposition freezing was observable. For the higher supercooling temperature interval deposition freezing was apparent but the counted number of ice crystals was very low. For the FROST measurement setup, therefore, deposition freezing was negligible.

Evaporation freezing could occur as the droplets generated in LACIS evaporate due to the Wegener-Bergeron-Findeisen effect. However, the one-section measurements clearly show that liquid droplets and ice crystals coexist. Because the droplet size distribution is narrow, the ice particles are most likely not formed by evaporation freezing (and also not through a condensation freezing process). In other words the ice formation observed is most likely due to immersion freezing processes. In addition, the smooth ice fraction behavior determined from the two-section measurements for $T_{\rm s}$

ACPD

9, 15827–15865, 2009

Measurements and parameterization of immersion freezing



laying between 32.5 K and 37.5 K is suggestive for the occurrence of a single heterogenous freezing mode, namely immersion freezing.

Finally, ice fraction values for all measured IN are presented in Fig. 9 for given LACIS supercooling temperatures. The ice fraction values increase with increasing supercooling temperature for all IN types, but in a different manner. Note again that the ice fraction values for $T_{\rm s}$ <34 K are underestimated because the supercooled droplets evaporate before reaching the adjusted wall temperature (see Fig. 3). However, the degree of underestimation should be similar for all kinds of IN, such that a comparison between the different IN materials can still be drawn.

Uncoated particles and those with $C_4H_6O_4$ coatings or with small amounts of H_2SO_4 (1) start to act as IN at lower T_s compared to particles with larger amounts H_2SO_4 (2) or with $(NH_4)_2SO_4$ coatings. For $T_s < 34$ K, pure ATD particles feature the largest IN capability. For $T_s \ge 35$ K, pure ATD particles and those coated with $C_4H_6O_4$, small and large amounts of H_2SO_4 seem to have a similar IN ability while particles coated with $(NH_4)_2SO_4$ are the most ineffective IN for the whole temperature range investigated.

The question remains which factors cause the difference in the freezing behavior. Several groups, including Hung et al. (2003) and Zobrist et al. (2008), found a freezing point depression for various aqueous solution droplets having mineral dust particles immersed. During FROST, the particles were coated with soluble substances which dissolve when the water condensed on the particles, so it is natural to consider whether the freezing process was related to water activity. Accompanying measurements on hygroscopic growth and activation were performed during the measurement campaign (see Wex et al., 2009) and provide information about that relation. In general, uncoated particles and those coated with small amounts of H_2SO_4 or with $C_4H_6O_4$, showed almost no hygroscopic growth. Particles coated with larger amounts of H_2SO_4 and with $(NH_4)_2SO_4$ grew measurably above 95% RH, showing a similar hygroscopic behavior. All types of particles were found to be activated at atmospherically relevant supersaturations (0.1 to 0.4%), with particles coated with larger amounts of H_2SO_4 and with $(NH_4)_2SO_4$ being most efficient CCN (Wex et al., 2009). Although the latter two cases

ACPD

9, 15827–15865, 2009

Measurements and parameterization of immersion freezing





showed similar hygroscopic growth and activation behavior, they differed in their ability to act as IN. This finding suggests that the investigated particle's ability to act as IN might not be related to water activity for the immersion freezing process investigated in this study. However, it should be noted that the supercooled droplets were activated and highly diluted before freezing occurred.

The simplified CNT parameterization (Eq. 8) presented in Sect. 2 was applied to determine the parameters a and $f_{\rm het}$ for all types of IN investigated. This parameterization can be used because the major part of ice is formed in the second section where the supercooling temperature is almost constant and therefore $j_{\rm het}$ is almost constant. The residence time within the last section is about 1.56 s. The determined parameters are presented in Table 1 and the corresponding curves are plotted in Fig. 10. Note that the ice fraction values for $T_{\rm s}$ <34 K were not used in the parameter determination since the ice fraction values are underestimated for these supercooling temperatures. Inserting the determined values for a and $f_{\rm het}$ into Eq. (4) and assuming that all types of particles are nearly spherical with a mass equivalent diameter of 300 nm the corresponding nucleation rates can be calculated (see Fig. 11). The nucleation rates are independent of the setup chosen and thus comparable with nucleation rates obtained by other methods.

It is obvious in Table 1 that both parameters, a and $f_{\rm het}$, change for the different types of IN. The factor $f_{\rm het}$ is smallest for pure ATD particles and highest for ATD particles coated with $({\rm NH_4})_2{\rm SO_4}$. That means that the energy barrier which has to be overcome so that a critical ice embryo can be initiated on the particle surface, is lowest for pure ATD particles and highest for ATD particles coated with $({\rm NH_4})_2{\rm SO_4}$. This suggests that surface properties have been altered, e.g., in the context of CNT, the interfacial free energy, or contact angle, has changed. Microscopically, this could be viewed as defects being blocked, changed or destroyed due to the coating procedure. It is plausible, for example, that the exposure of the sulfuric acid to water vapor, which occurs during the addition of ammonia to form $({\rm NH_4})_2{\rm SO_4}$, accelerates the reaction with the mineral dust, thereby leading to the greatest reduction in nucleating efficiency (Lasaga, 1995).

ACPD

9, 15827–15865, 2009

Measurements and parameterization of immersion freezing





Microscopic alteration of the surface can perhaps be expressed in terms of active sites (an active site is a preferred site which is comparable in size to critical embryo and where free energy of particle-ice interface is as small as possible (Fletcher, 1969; Vali, 2008)), but doing this would require some knowledge of the distribution of active site properties, which at this time are uncharacterized.

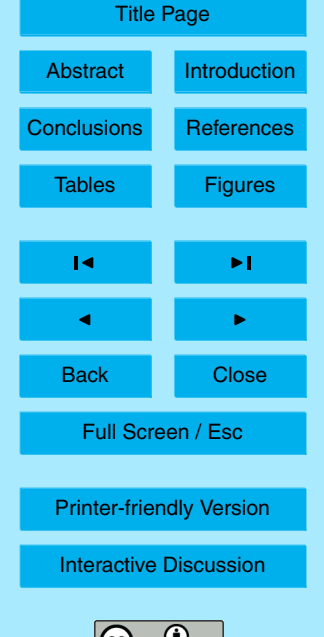
Concerning parameter a, the lowest value is also obtained for pure ATD particles and the highest value for ATD coated with large amounts of H_2SO_4 , in spite of the fact that this trend goes against the change in nucleation rate (i.e., nucleation rate decreases, although a increases). Since a includes information about total particle surface and kinetic effects, the increase can be interpreted as an increased surface area per particle, or as an increase in the rate at which molecules can be transferred from the liquid to ice. Since both values, a and f_{het} , change in comparable manner, but with opposite tendencies for the nucleation rate, it appears that the thermodynamic effect is most dominant for the change in immersion freezing behavior resulting from coating processes.

The determined ice fraction values seem to be somewhat low for the temperature region investigated. This results from the fact that monodisperse particles were used (no large particles contributing to "early" onset of freezing), and because of the low residence time inside LACIS. The parameterization, developed in this work, can also be used to derive ice fraction values for higher residence times. In Fig. 12, the ice fraction curves for three different residence times are shown. It is clearly seen that the residence time largely influences the number of ice crystals formed. Due to this dependency it becomes obvious that ice fractions determined with different measurement setups are not comparable. Instead, nucleation rates (as given in Fig. 11) have to be considered when comparing the results from different investigations featuring e.g. different residence and/or temperatures.

ACPD

9, 15827–15865, 2009

Measurements and parameterization of immersion freezing



5 Conclusions

During the measurement campaign FROST, which took place in April 2008, LACIS was used to investigate the ability of size-segregated, coated and uncoated mineral dust particles to act as IN in the immersion mode. These were the first measurements of heterogenous freezing performed with LACIS. For experiments a surrogate of mineral dust, namely Arizona Test Dust, was used. The particles were also coated with various types of substances such as ammonium sulfate ((NH₄)₂SO₄), sulfuric acid (H_2SO_4) , two different coating conditions) and succinic acid $(C_4H_6O_4)$. For the freezing experiments a quasi-monodisperse particle size distribution with a mobility diameter of 300 nm was chosen. Additional instrumentation was used to characterize the selected particles with respect to shape, chemical composition, hygroscopic growth and droplet activation (Wex et al., 2009; Reitz et al., 2009). At LACIS, various temperature values between 233.15 K and 240.65 K were adjusted and the corresponding ice fraction values were determined. In this temperature range, uncoated particles and those coated with C₄H₆O₄ or small amounts of H₂SO₄ act as IN at higher temperatures compared to particles with larger amounts of H₂SO₄ or (NH₄)₂SO₄ coatings. Although the latter two showed similar hygroscopic growth and droplet activation behavior, they differed in their ability to act as IN, with ATD particles coated with (NH₄)₂SO₄ being the most ineffective IN. It seems that the ability of the investigated particles to act as IN is not related to water activity for the freezing process investigated. However, it should be noted that the supercooled droplets were activated and highly diluted when the freezing occurred.

Based on classical nucleation theory and assuming a stochastic freezing process a parameterization was developed to describe the influence of the different particles on immersion freezing. The parameterization shows that due to the coating the energy barrier, which has to be overcome that freezing can occur, is increased. The reason may be that the particle surface is modified due to the coating. Furthermore, the parameterization suggests that the total particle surface and/or kinetic effects are also changed due to the coating procedure. But it appears that the thermodynamic effect

ACPD

9, 15827–15865, 2009

Measurements and parameterization of immersion freezing



is most dominant for the change in immersion freezing behavior resulting from coating processes.

The parameterization was also used to derive ice fraction values for higher residence times. It clearly demonstrates that the residence time largely influences the amount of frozen particles. Due to this dependency, ice fractions determined with different measurement setups are not comparable. Instead, nucleation rates have to be considered which can be generally compared.

Acknowledgements. The measurement campaign FROST was conducted within the Helmholtz Virtual Institute "Aerosol-Cloud Interactions" funded by the Helmholtz society. This work is part of a DFG project under contract HE 939/21-1. Additionally, the campaign was financially supported by the research project EUROCHAMP funded within the EC 6th Framework Program, Section "Support for Research Infrastructures – Integrated Infrastructure Initiative". RAS acknowledges support from the Alexander von Humboldt Foundation during the time this research was carried out.

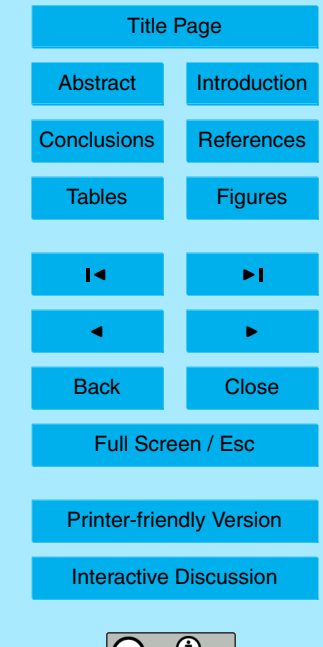
References

- Archuleta, C. M., DeMott, P. J., and Kreidenweis, S. M.: Ice nucleation by surrogates for atmospheric mineral dust and mineral dust/sulfate particles at cirrus temperatures, Atmos. Chem. Phys., 5, 2617–2634, 2005,
 - http://www.atmos-chem-phys.net/5/2617/2005/. 15830
- Cantrell, W. and Heymsfield, A.: Production of ice in tropospheric clouds a review, B. Am. Meteorol. Soc., 86(6), 795–807, 2005. 15829, 15830
- Cziczo, D. J., Murphy, D. M., Hudson, P. K., and Thomson, D. S.: Single particle measurements of the chemical composition of cirrus ice residue during crystal-face, J. Geophys. Res.-Atmos., 109, D04201, doi:10.1029/2003JD004032, 2004. 15830
- DeMott, P. J., Cziczo, D. J., Prenni, A. J., Murphy, D. M., Kreidenweis, S. M., Thomson, D. S., Borys, R., and Rogers, D. C.: Measurements of the concentration and composition of nuclei for cirrus formation, Proceedings of the National Academy of Sciences of the United States of America, 100(25), 14655–14660, 2003a. 15830

ACPD

9, 15827–15865, 2009

Measurements and parameterization of immersion freezing

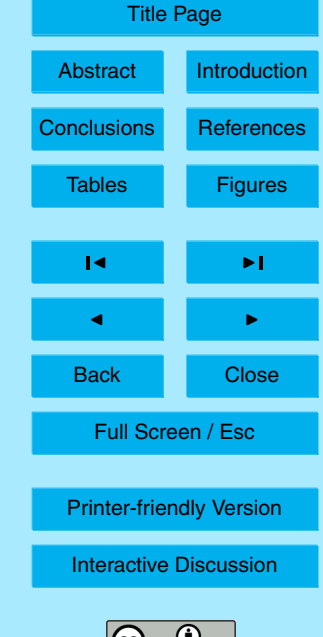




- DeMott, P. J., Sassen, K., Poellot, M. R., Baumgardner, D., Rogers, D. C., Brooks, S. D., Prenni, A. J., and Kreidenweis, S. M.: African dust aerosols as atmospheric ice nuclei, Geophys. Res. Lett., 30(14), 1732, doi:10.1029/2003GL017410, 2003b. 15828, 15830
- Durant, A. J. and Shaw, R. A.: Evaporation freezing by contact nucleation inside-out, Geophys. Res. Lett., 32, L20814, doi:10.1029/2005GL024175, 2005. 15829
- Field, P. R., Möhler, O., Connolly, P., Krämer, M., Cotton, R., Heymsfield, A. J., Saathoff, H., and Schnaiter, M.: Some ice nucleation characteristics of Asian and Saharan desert dust, Atmos. Chem. Phys., 6, 2991–3006, 2006,
 - http://www.atmos-chem-phys.net/6/2991/2006/. 15830
- Findeisen, W.: Die kolloidmeteorologischen Vorgänge bei der Niederschlagsbildung, Meteorologische Zeitung, 55, 121–133, 1938. 15842
 - Fletcher, N. H.: Active sites and ice crystal nucleation, J. Atmos. Sci., 26(6), 1266–1271, 1969. 15846
 - FLUENT: FLUENT 6 user's guide, FLUENT Inc., 2001. 15838
- Hartmann, S., Niedermeier, D., Shaw, R., Wex, H., and Stratmann, F.: Immersion freezing studies at the leipzig Aerosol Cloud Interaction Simulator, in preparation, 2009. 15834, 15838, 15839, 15842
 - Hennig, T., Massling, A., Brechtel, F. J., and Wiedensohler, A.: A tandem DMA for highly temperature-stabilized hygroscopic particle growth measurements between 90% and 98% relative humidity, J. Aerosol Sci., 36, 1210–1223, 2005. 15836
 - Hirst, E., Kaye, P. H., Greenaway, R. S., Field, P., and Johnson, D. W.: Discrimination of micrometer-sized ice and super-cooled droplets in mixed-phase cloud, Atmos. Environ., 35, 33–47, 2001.
 - Hung, H. M., Malinowski, A., and Martin, S. T.: Kinetics of heterogeneous ice nucleation on the surfaces of mineral dust cores inserted into aqueous ammonium sulfate particles, J. Phys. Chem. A. 107(9), 1296–1306, 2003, 15828, 15844
 - Kärcher, B. and Lohmann, U.: A parameterization of cirrus cloud formation: Heterogeneous freezing, J. Geophys. Res.-Atmos., 108, 4402, doi:10.1029/2002JD003220, 2003. 15830
 - Kiselev, A., Wex, H., Stratmann, F., Nadeev, A., and Karpushenko, D.: White-light optical particle spectrometer for in situ measurements of condensational growth of aerosol particles, Appl. Optics, 44(22), 4693–4701, 2005.
 - Knopf, D. A. and Koop, T.: Heterogeneous nucleation of ice on surrogates of mineral dust, J. Geophys. Res.-Atmos., 111, D12201, doi:10.1029/2005JD006894, 2006. 15830

9, 15827–15865, 2009

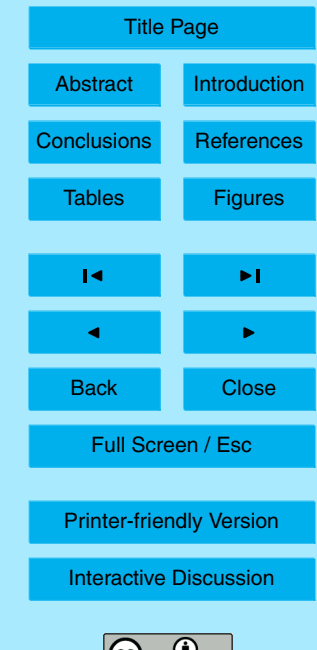
Measurements and parameterization of immersion freezing



- Knutson, E. O. and Whitby, K. T.: Aerosol classification by electric mobility: Apparatus, theory and applications, J. Aerosol Sci., 6, 443–451, 1975. 15836
- Lasaga, A. C.: Fundamental approaches in describing mineral dissolution and precipitation rates, in: Chemical Weathering Rates of Silicate Minerals, volume 31 of Reviews in Mineralogy, pages 23–86. Mineralogical Society America, Washington, USA, 1995. 15845
- Lohmann, U.: Aerosol effects on clouds and climate, pages 129-137, 2006. 15829
- Marcolli, C., Gedamke, S., Peter, T., and Zobrist, B.: Efficiency of immersion mode ice nucleation on surrogates of mineral dust, Atmos. Chem. Phys., 7, 5081–5091, 2007, http://www.atmos-chem-phys.net/7/5081/2007/. 15830
- Megahed, K.: The Impact of Mineral Dust Aerosol Particles on Cloud Formation, Dissertation, Rheinischen Friedrich-Wilhelms-Universität Bonn, 2007. 15829
 - Mertes, S., Galgon, D., Schwirn, K., Nowak, A., Lehmann, K., Massling, A., Wiedensohler, A., and Wieprecht, W.: Evolution of particle concentration and size distribution observed upwind, inside and downwind hill cap clouds at connected flow conditions during FEBUKO, Atmos. Environ., 39, 4233–4245, 2005. 15831
 - Meyers, M. P., Demott, P. J., and Cotton, W. R.: New primary ice-nucleation parameterizations in an explicit cloud model, J. Appl. Meteorol., 31(7), 708–721, 1992. 15829
 - Möhler, O., Field, P. R., Connolly, P., Benz, S., Saathoff, H., Schnaiter, M., Wagner, R., Cotton, R., Krämer, M., Mangold, A., and Heymsfield, A. J.: Efficiency of the deposition mode ice nucleation on mineral dust particles, Atmos. Chem. Phys., 6, 3007–3021, 2006, http://www.atmos-chem-phys.net/6/3007/2006/. 15830
 - Particle Dynamics: FPM User's Guide, www.particle-dynamics.de, Particle Dynamics GmbH, Leipzig, Germany, 2005. 15838
 - Prospero, J. M.: Long-term measurements of the transport of African mineral dust to the southeastern United States: Implications for regional air quality, J. Geophys. Res.-Atmos., 104(D13), 15917–15927, 1999. 15830
 - Pruppacher, H. R. and Klett, J. D.: Microphysics of Clouds and Precipitation, Kluwer Academic Publishers, Dordrecht, The Netherlands, 1997. 15829, 15832, 15834
 - Reitz, P., Schneider, J., Wex, H., Startmann, F., Niedermeier, D., Mildenberger, K., Covert, D., Spindler, C., Mentel, T. F., Poulain, L., and Borrmann, S.: Detection of thin coatings on refractory particles with an aerodyne aerosol mass spectrometer and implications for laboratory studies of hygroscopic growth, CCN and IN activation, in preparation, 2009. 15831, 15847 Richardson, M. S., DeMott, P. J., Kreidenweis, S. M., Cziczo, D. J., Dunlea, E. J., Jimenez,

9, 15827–15865, 2009

Measurements and parameterization of immersion freezing



- J. L., Thomson, D. S., Ashbaugh, L. L., Borys, R. D., Westphal, D. L., Casuccio, G. S., and Lersch, T. L.: Measurements of heterogeneous ice nuclei in the western united states in springtime and their relation to aerosol characteristics, J. Geophys. Res.-Atmos., 112, D02209. doi:10.1029/2006JD007500, 2007. 15830
- ⁵ Roberts, G. C. and Nenes, A.: A continuous-flow streamwise thermal-gradient CCN chamber for atmospheric measurements, Aerosol Sci. Technol., 39(3), 206–221, 2005. 15836
 - Rogers, R. and Yau, M.: A Short Course in Cloud Physics, volume 3, Butterworth Heinemann-An imprint of Elsevier, third edition, 1996. 15833
 - Sassen, K., DeMott, P. J., Prospero, J. M., and Poellot, M. R.: Saharan dust storms and indirect aerosol effects on clouds: Crystal-face results, Geophys. Res. Lett., 30, 1633, doi:10.1029/2003GL017371, 2003. 15830
 - Seinfeld, J. and Pandis, S.: Atmospheric Chemistry and Physics From Air Pollution to Climate Change, Wiley-Interscience, 1998. 15832
 - Shaw, R. A., Durant, A. J., and Mi, Y.: Heterogeneous surface crystallization observed in undercooled water, J. Phys. Chem. B, 109, 9865–9868, 2005. 15829, 15832, 15834
 - Stratmann, F., Kiselev, A., Wurzler, S., Wendisch, M., Heintzenberg, J., Charlson, R. J., Diehl, K., Wex, H., and Schmidt, S.: Laboratory studies and numerical simulations of cloud droplet formation under realistic supersaturation conditions, J. Atmos. Oceanic Technol., 21(6), 876–887, 2004. 15831
- Vali, G.: Freezing rate due to heterogneous nucleation, J. Atmos. Sci., 51(13), 1843–1856, 1994.
 - Vali, G.: Repeatability and randomness in heterogeneous freezing nucleation, Atmos. Chem. Phys., 8, 5017–5031, 2008, http://www.atmos-chem-phys.net/8/5017/2008/. 15846
- Wex, H., Clauss, T., Covert, D., Hallbauer, E., Hartmann, S., Kiselev, A., Mentel, T. F., Mildenberger, K., Niedermeier, D., Poulain, L., Reitz, P., Schneider, J., Shaw, R., Spindler, C., and Stratmann, F.: Classifying coated and uncoated arizona test dust with respect to hygroscopic growth and activation, in preparation, 2009. 15831, 15834, 15844, 15847
 - Yuskiewicz, B. A., Stratmann, F., Birmili, W., Wiedensohler, A., Swietlicki, E., Berg, O., and Zhou, J.: The effects of in-cloud mass production on atmospheric light scatter, Atmos. Res., 50, 265–288, 1999. 15831
 - Zobrist, B., Koop, T., Luo, B. P., Marcolli, C., and Peter, T.: Heterogeneous ice nucleation rate coefficient of water droplets coated by a nonadecanol monolayer, J. Phys. Chem. C, 111(5),

9, 15827–15865, 2009

Measurements and parameterization of immersion freezing



- 2149-2155, 2007, 15833
- Zobrist, B., Marcolli, C., Peter, T., and Koop, T.: Heterogeneous ice nucleation in aqueous solutions: the role of water activity, J. Phys. Chem. A, 112(17), 3965–3975, 2008. 15830, 15844
- ⁵ Zuberi, B., Bertram, A. K., Cassa, C. A., Molina, L. T., and Molina, M. J.: Heterogeneous nucleation of ice in (NH₄)₂SO₄-H₂O particles with mineral dust immersions, Geophys. Res. Lett., 29(10), 1504, doi:10.1029/2001GL014289, 2002. 15828, 15830

9, 15827–15865, 2009

Measurements and parameterization of immersion freezing

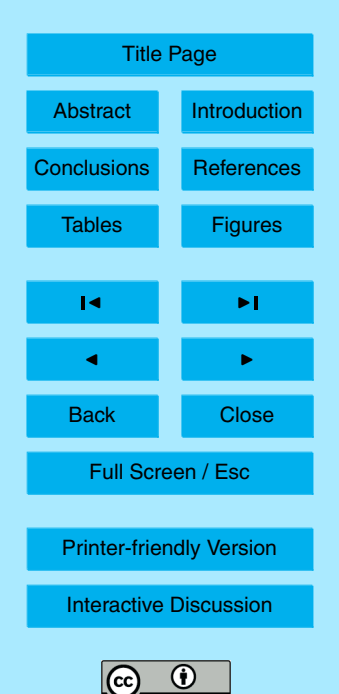


Table 1. Parameters a and f_{het} for the immersion freezing of supercooled water droplets containing different types of IN.

Particle Type	a [s ⁻¹]	f _{het}
ATD	1.31E+00	4.51E-02
ATD+C ₄ H ₆ O ₄	8.46E+00	6.83E-02
ATD+H ₂ SO ₄ (1)	1.57E+01	7.79E-02
ATD+H ₂ SO ₄ (2)	5.71E+02	1.35E-01
ATD+(NH ₄) ₂ SO ₄	1.31E+02	1.40E-01

9, 15827–15865, 2009

Measurements and parameterization of immersion freezing

Title Page		
Abstract	Introduction	
Conclusions	References	
Tables	Figures	
Id	►I	
4	•	
Back	Close	
Full Screen / Esc		
Printer-friendly Version		
Interactive Discussion		

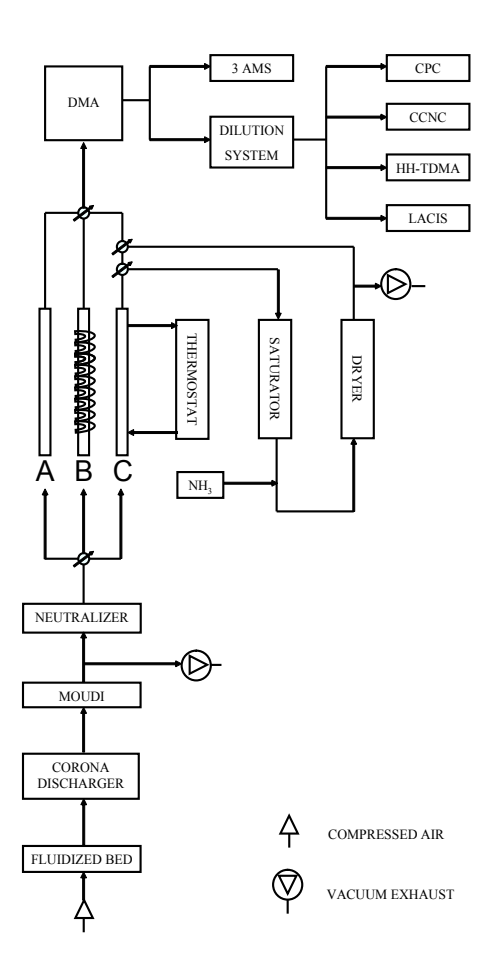
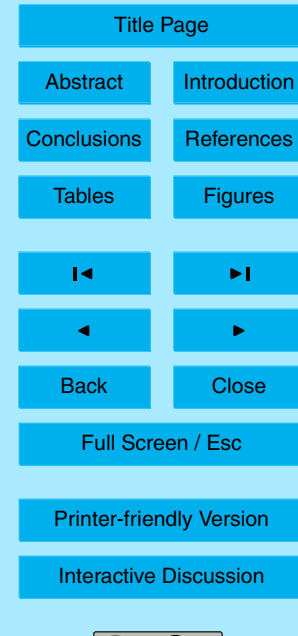


Fig. 1. Sketch of the generation, coating and size selection of the particles. Also included are the different measurement instruments which measured during FROST.

9, 15827-15865, 2009

Measurements and parameterization of immersion freezing





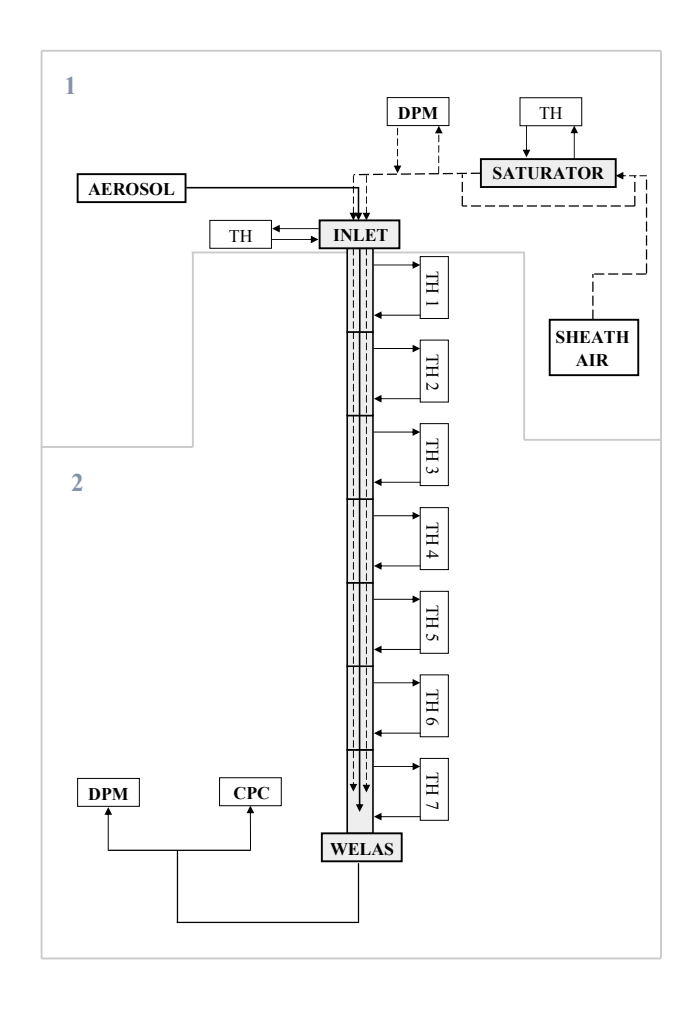


Fig. 2. Setup of particle conditioning (1) and LACIS flow tube (2).

15855

ACPD

9, 15827-15865, 2009

Measurements and parameterization of immersion freezing





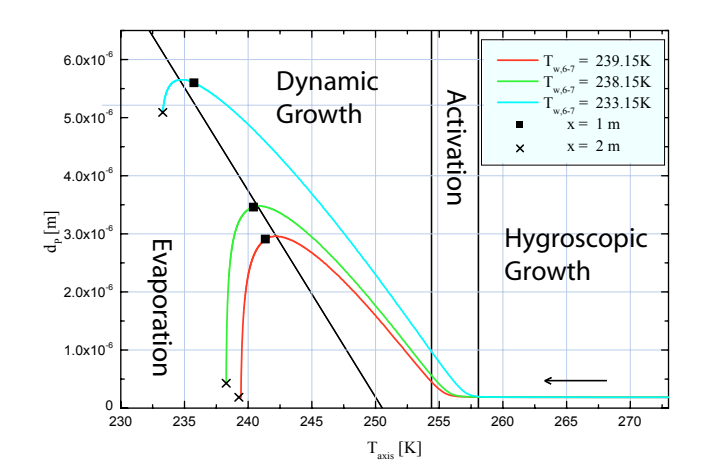


Fig. 3. FLUENT/FPM model simulations of the droplet growth behavior inside the last two sections for three different wall temperatures (233.15 K, 238.15 K and 239.15 K). $T_{\rm axis}$ is the temperature which the particles experience in the particle beam. The curves are traced from right to left as particles cool monotonically while moving along the axis of the LACIS flow tube. The black square and cross represent the droplet size after the first and second freezing section.

9, 15827–15865, 2009

Measurements and parameterization of immersion freezing



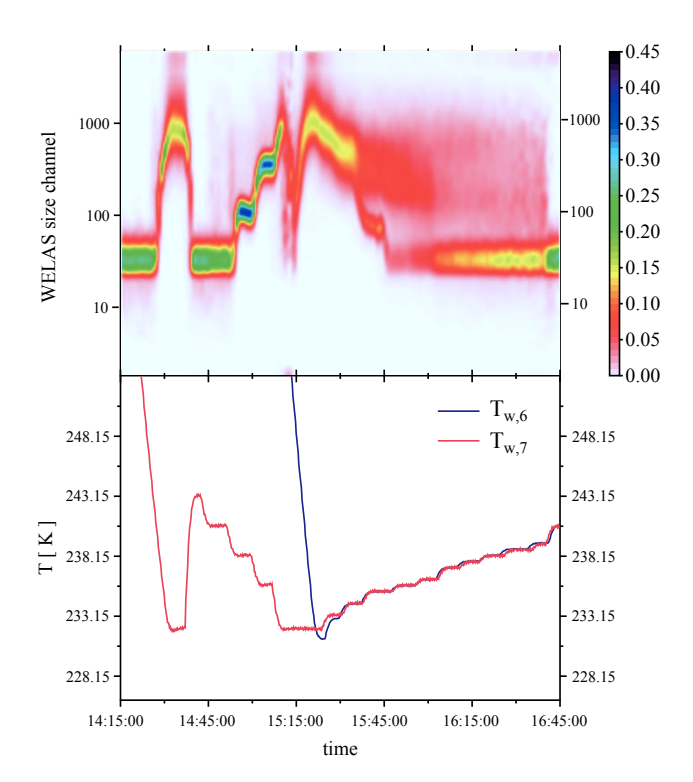
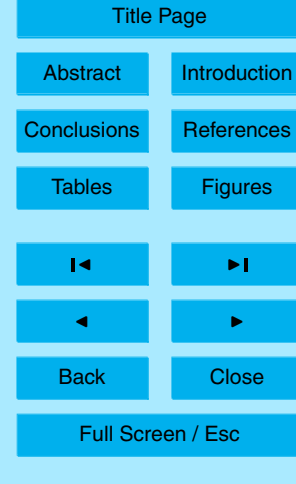


Fig. 4. In the upper panel, a contour plot is given, presenting the time series of measured size distributions during a cooling cycle. The color represents the normalized number. The corresponding wall temperatures of Sects. 6 and 7 are shown in the lower panel. Note, that the size dependent counting efficiency of WELAS[®] data is not considered.

9, 15827-15865, 2009

Measurements and parameterization of immersion freezing

D. Niedermeier et al.



Interactive Discussion

Printer-friendly Version



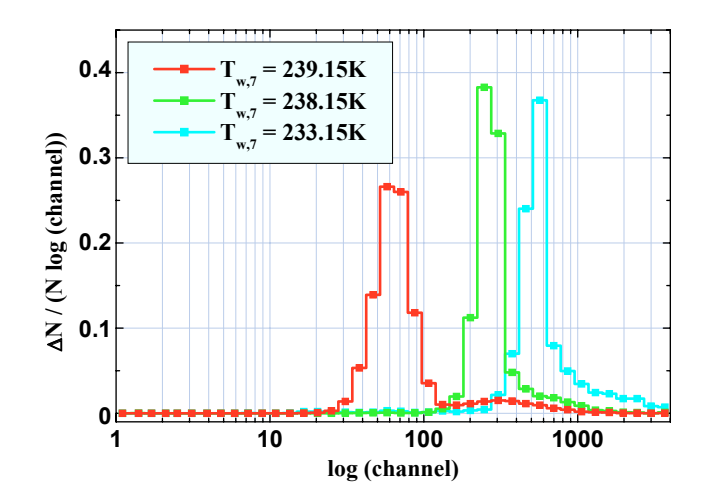
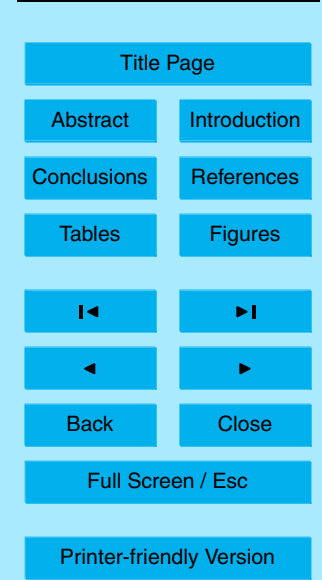


Fig. 5. Particle size distributions as result of a one-section measurement for three different wall temperature settings. The normalized number is plotted versus the logarithm of WELAS® size channel. The narrow modes are caused by supercooled liquid water droplets, while the tails originate from ice crystals.

9, 15827-15865, 2009

Measurements and parameterization of immersion freezing

D. Niedermeier et al.





Interactive Discussion

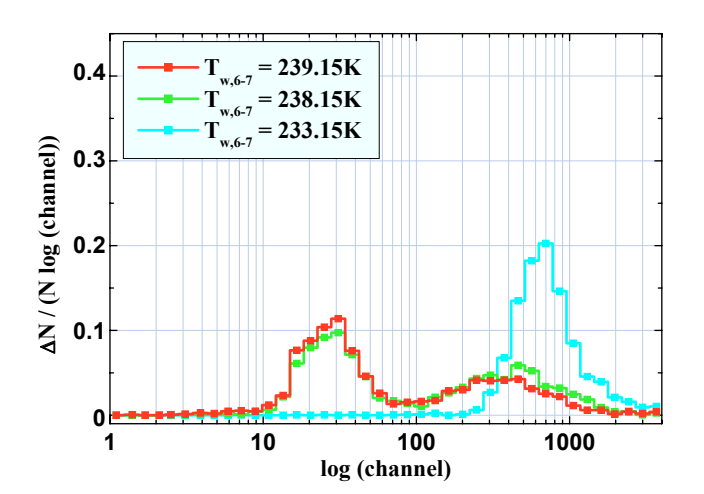
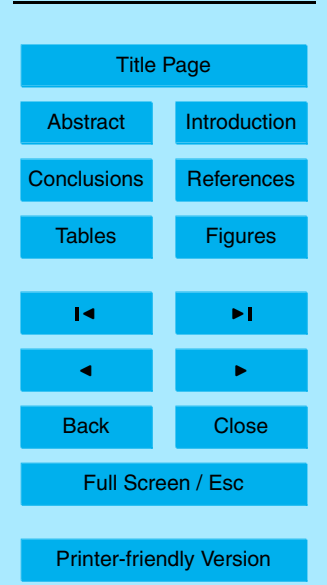


Fig. 6. Particle size distributions as result of a two-section measurement for three different wall temperature settings. The normalized number is plotted versus the logarithm of WELAS® size channel. The mode below channel 100 is the seed mode. The broad modes above channel 100 are ice crystal modes. In contrast to one-section measurement supercooled liquid droplets are absent.

9, 15827–15865, 2009

Measurements and parameterization of immersion freezing

D. Niedermeier et al.





Interactive Discussion

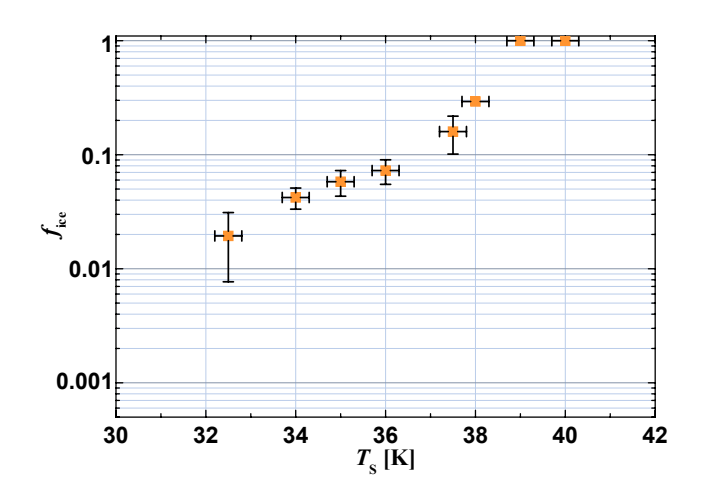
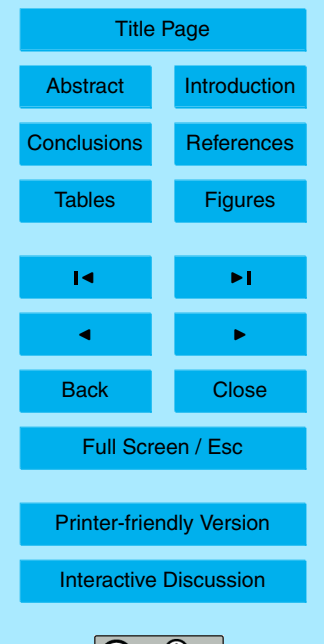


Fig. 7. Ice fraction of pure ATD for different supercooling temperatures T_s .

9, 15827-15865, 2009

Measurements and parameterization of immersion freezing



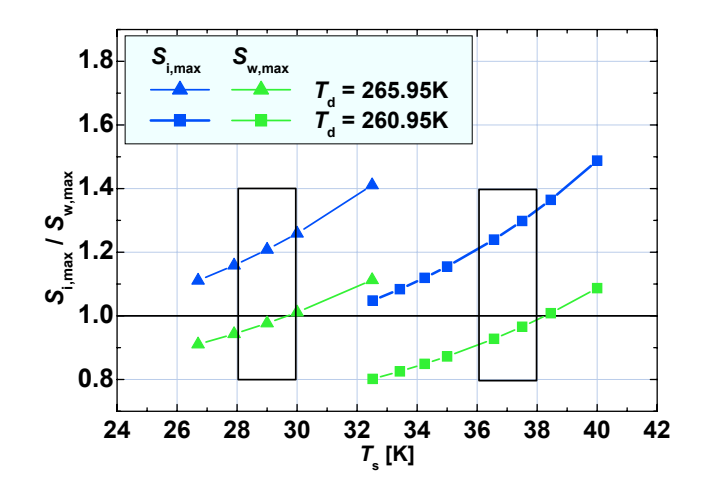
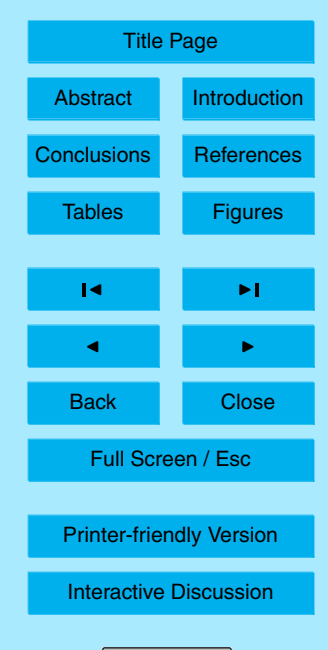


Fig. 8. FLUENT/FPM model simulations for LACIS adjustments to measure possible deposition freezing. The maximum saturation ratios with respect to ice (blue) and liquid water (green) are plotted versus $T_{\rm s}$ for two different inlet dew-points (265.95 K (triangle) and 260.95 K (square)). The black boxes represent the measurement region.

9, 15827-15865, 2009

Measurements and parameterization of immersion freezing



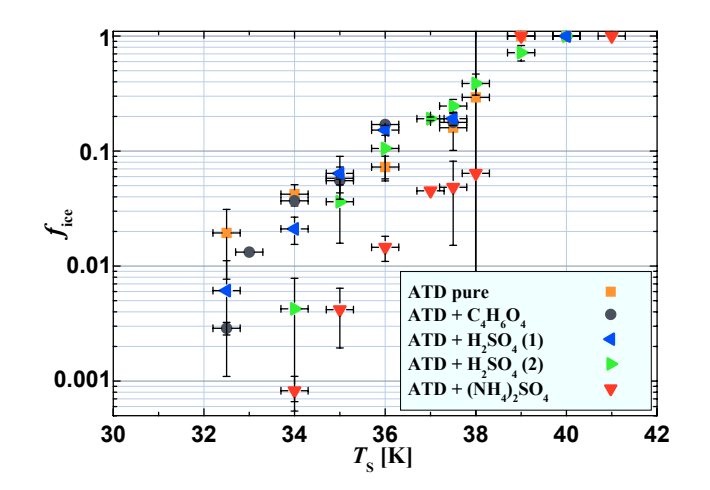


Fig. 9. Immersion freezing behavior of all types of particles. The determined ice fraction $f_{\rm ice}$ is plotted versus the supercooling temperature $T_{\rm s}$. The line at $T_{\rm s}$ =38 K separates the heterogeneous (on the left) and homogeneous (on the right) freezing modes.

9, 15827–15865, 2009

Measurements and parameterization of immersion freezing

D. Niedermeier et al.

Title Page

Thie Tage		
Introduction		
References		
Figures		
►I		
•		
Close		
Full Screen / Esc		
Printer-friendly Version		
Interactive Discussion		

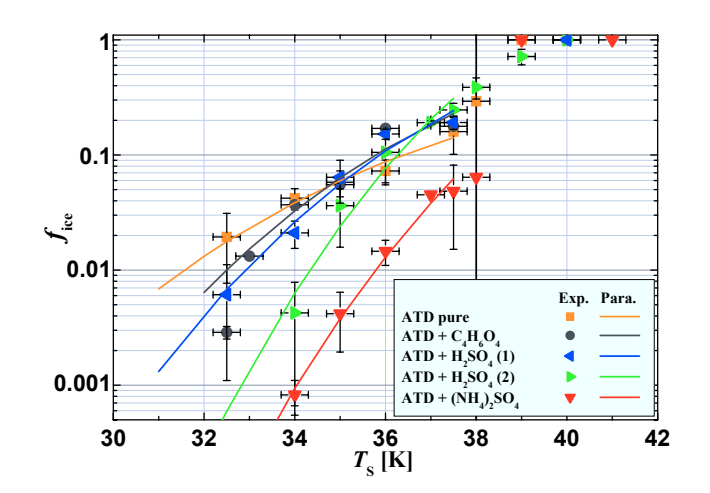
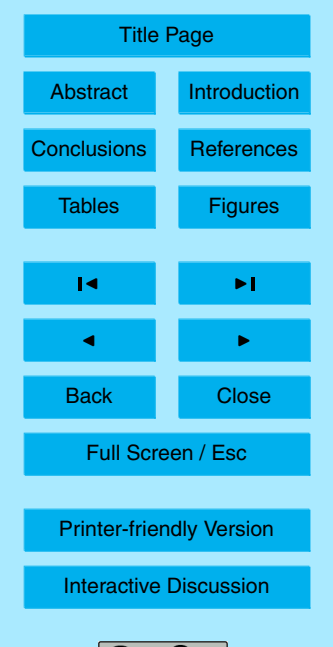


Fig. 10. Immersion freezing behavior of all types of particles. The determined ice fraction values $f_{\rm ice}$ and the parameterization curves are plotted. The line at $T_{\rm s}$ =38 K separates the heterogeneous (on the left) and homogeneous (on the right) freezing modes.

9, 15827-15865, 2009

Measurements and parameterization of immersion freezing



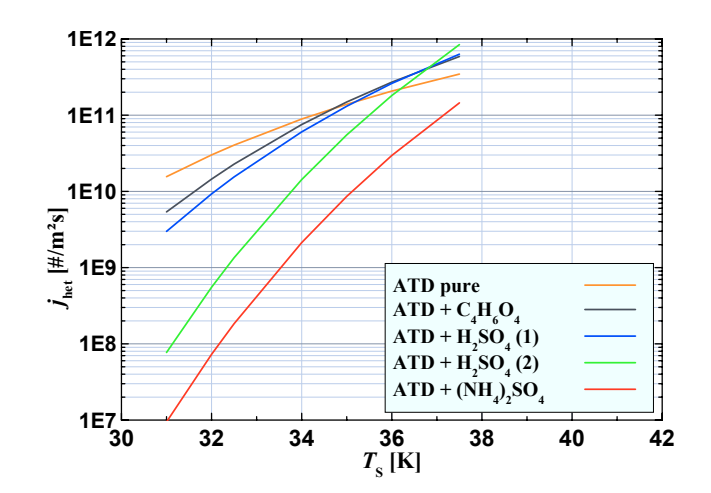
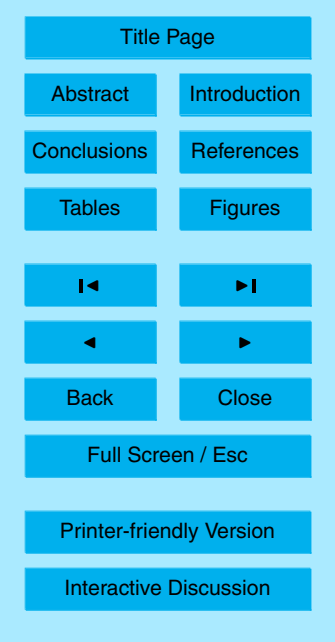


Fig. 11. Nucleation rates j_{het} for all types of particles. For the determination of j_{het} , the values for a and f_{het} are inserted into Eq. (4) and all types of IN are assumed to be spherical with a mass equivalent diameter of 300 nm.

9, 15827–15865, 2009

Measurements and parameterization of immersion freezing



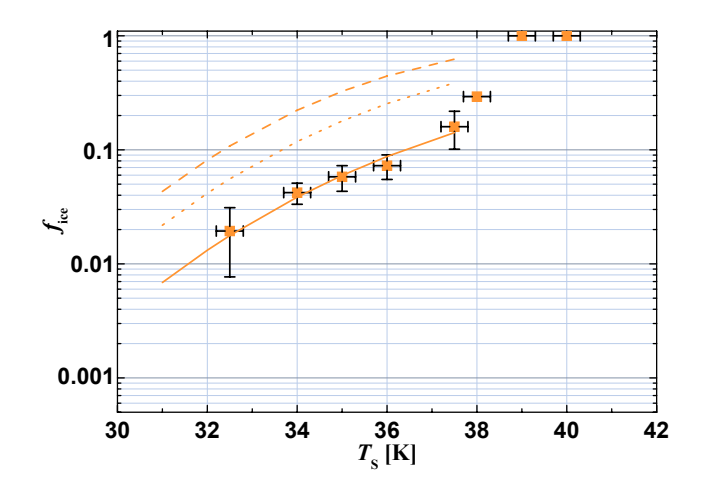


Fig. 12. Freezing behavior of pure ATD particles. Additionally, parameterization curves for three different residence times (dashed line: 10 s, dotted line: 5 s and solid line: 1.56 s) are inserted.

9, 15827–15865, 2009

Measurements and parameterization of immersion freezing

